Orbital
The electronic journal of chemistry

the electronic journal of chemistry

Full Paper | http://dx.doi.org/10.17807/orbital.v17i5.20094

Adsorption of Methylene Blue Using the Biosorbent of Teak Sawdust

Anselmus Boy Baunsele*[a], Dwi Siswanta[b], Hildegardis Missa[c], Merpiseldin Nitsae[d], Johnson Nune Naat[e], Abner Tonu Lema[f], Fidelis Nitti[g], and Jafar La Kilo[h]

The expansion of the textile industry on a global scale has led to a decline in the quality of our environment due partly to the increasing discharge of untreated textile waste. Industrial textile waste generates two types of environmental pollution-heavy metals and dyes; both possess mutagenic and carcinogenic properties. While efforts have been made to reduce the negative effects of dyes, adsorption remains one of the most cost-effective and effective method. In this context, teak wood sawdust, a readily available byproduct of carpentry activities, was investigated as a potential biosorbent for the removal of methylene blue from aqueous solution. The inherent present of cellulose, hemicellulose, and lignin in teak sawdust make it an ideal biosorbent. The physicochemical properties and surface functionalities of the biosorbent were characterized using Fourier Transform Infrared Spectroscopy (FTIR) and Scanning Electron Microscopy-Energy Dispersive X-ray Spectroscopy (SEM-EDX). This study uses the UV-Vis Spectrophotometer measurement method to determine the effect of pH, contact time, and concentration on methylene blue's adsorption capacity. The optimal conditions for the adsorption were identified at pH 6, with an equilibrium time of 30 minutes and an initial methylene blue concentration of 30 ppm. Under these conditions, the adsorption efficiency reached 99.40%. Kinetic modeling revealed that the adsorption process followed a pseudo-second-order model, with a rate constant of 79.70 g mg^{-1} min^{-1}. The maximum adsorption capacity was determined to be 1.351 mg g^{-1}, and the process achieved a methylene blue removal efficiency of 99.79%, with a Freundlich isotherm constant (n) value of 1, indicating favorable adsorption characteristics.

Graphical abstract

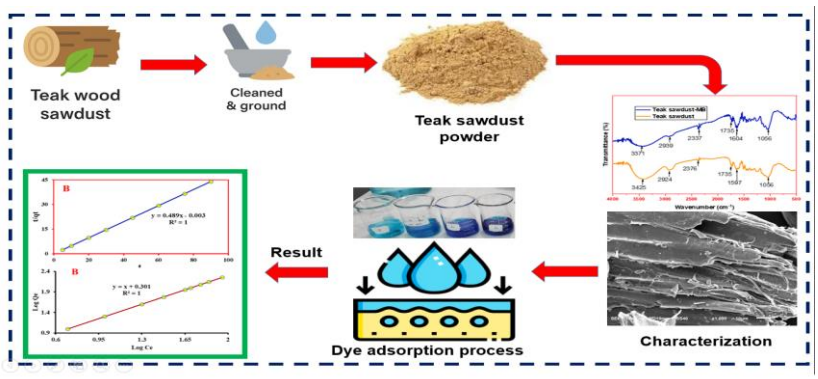

Keywords

Adsorption
Biosorbent
Teak Wood Sawdust
Isothermal
Kinetic
Methylene blue

Article history

Received 23 Jan 2024
Revised 16 Jul 2025
Accepted 08 Sep 2025
Available online 22 Nov 2025

Handling Editor: Vania D. Schwade

[a]Chemistry Education Department, Faculty of Education and Teachers Training, Widya Mandira Catholic University, Kupang (85225), East Nusa Tenggara, Indonesia. [b]Department of Chemistry, Faculty of Mathematics and Natural Sciences, Gadjah Mada University, Yogyakarta (55281), Indonesia. [c]Biology Education Department, Faculty of Education and Teachers Training, Widya Mandira Catholic University, Kupang (85225), East Nusa Tenggara, Indonesia. *Continued on the next page.*

1. Introduction

The rapid expansion in industrial activities in recent years has led to significant environmental damage, posing a serious pollution problem on a global scale. A major contributing factor to this issue is the discharge of substantial volume of untreated waste by industries worldwide. Despite the urgent need for proper waste management, many industries sectors fail to implement adequate treatment process prior to waste disposal, which is imperative to preserve ecological equilibrium and protect environmental health. Industrial effluents, particularly those originating from large-scale and medium-scale manufacturing operations, often contain hazardous contaminants such as heavy metals and synthetic dyes [1]. These types of pollutants have the potential to bioaccumulate in the environment, posing serious threat to human health such as cancer, nerve damage, and even death [2]. Among the various industrial sectors, the textile industry stands out as a major contributor to dye pollution and industrial effluent generation.

A wide range of synthetic dyes, such as rhodamine B, methyl orange, and methylene blue, are widely used in industrial processes; however, their extensive application raises significant environmental and public health concerns. One of the major ecological impact is their ability to block sunlight penetration into the aquatic systems, thereby inhibiting photosynthetic activity in aquatic plants and increasing mortality rates among fish and other aquatic organisms [3]. Additionally, many of these dyes exhibit carcinogenic and mutagenic properties, with prolonged exposure and bioaccumulation potentially contributing to the onset of cancer and other chronic health conditions in human [4]. Both cationic and anionic dyes have been associated with various health issues, including cyanosis, vomiting, nerve damage, and an increased heart rate [5]. The environmental persistence of these dyes is largely attributed to their complex molecular structures, which exhibit significant resistant to thermal, photolytic and microbial degradation [6]. A notable example is congo red, a commonly used anionic dye in the textile industry, which has been associated with dermatological irritation and adverse effects on the liver, kidneys, and nervous system, with prolonged exposure may also lead to respiratory disorders [7]. Similarly, methylene blue, a widely used cationic dye, has been documented to cause skin irritation, irreversible ocular damage, cyanosis, nausea, neurotoxic effects, and tachycardia, thereby posing substantial risks to human health [8,9]. Given the toxicity and persistence of such dyes, the development and implementation of effective treatment strategies for industrial wastewater containing methylene blue are essential to prevent environmental and health hazards.

Given the environmental and health risks associated with dye pollution, particularly the improper treatment of wastewater containing methylene blue, various treatment methods have been developed. These include photocatalytic degradation techniques utilizing silver nanoparticle catalysts [10], electroflotation technique employing TiO_2 catalysts [11], electrochemical degradation using carbon-PVC electrodes [12], microbial biodegradation [4], and adsorption using various adsorbent materials [13]. Among these, adsorption has emerged as the most promising method due to its cost-effectiveness, operational simplicity, and high efficiency [14]. A wide range of naturally occurring materials has been explored as low-cost adsorbent sources, including agricultural and plant based wastes such as sugar cane bagasse [15], coconut fiber [16,17,18], palm fruit husks [19,20], used tea leaves [21], clove leaves [22], and peanut shells [23].

The purpose of this study was to explore the use teak sawdust as an adsorbent for the removal of methylene blue aqueous solution. Teak plants grow abundantly on Timor Island, especially in Kupang City, East Nusa Tenggara province of Indonesia, where the tropical climate conditions provides favorable conditions for their growth [24], leading to an abundant supply of teak sawdust waste from various furniture industries. Despite its abundance, this waste is usually just burnt without undergoing any special treatment. Previous studies have highlighted the potential value of teak plant byproducts; for instance, teak leaves as potential adsorbents [25], teak stems as a source for activated carbon [26,27]. Teak leaf extract is known for its antibacterial and anticancer properties [28], while teak wood is a valuable source of carbon [29]. In this context, the present study seeks to use the teak sawdust as low-cost adsorbent for the removal of methylene blue from aqueous solution. The adsorption performance was evaluated under varying experimental parameters, including solution pH, adsorption time, and initial dye concentration. Furthermore, adsorption kinetics and isotherm models were also employed to analyze the mechanism of interaction between methylene blue and teak sawdust adsorbents.

2. Material and Methods

2.1 Materials and Instrumentation

The adsorbent materials used in this study was prepared from teak wood sawdust, which was obtained from local furniture industries in Kupang City furniture. The chemicals used in this study included sodium hydroxide (NaOH) (Merk, purity of ≥99%), hydrochloric acid (HCl)(Merk, purity of 35-38%), Milli-Q Water (Ultrapure). Methylene blue (MB) ($C_{16}H_{18}N_3SCl$) (Merck, purity of ≥82%), with a molecular weight of 319.85 g mol^{-1}, was selected due to its widespread use in industrial textile and well-known for its environmental impacts. The molecular structure of MB is presented in Figure 1.

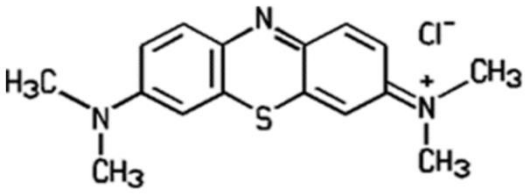

Fig. 1. The molecular structure of the methylene blue

[d]Biology Education Department, Faculty of Teachers Training and Education, Satya Wacana Christian University, Kupang (85228), East Nusa Tenggara, Indonesia. [e]Chemistry Education Department, Faculty of Education and Teachers Training, Nusa Cendana University, Kupang (85001), East Nusa Tenggara, Indonesia. [f]State Agricultural Polytechnic, Kupang, East Nusa Tenggara, (85001), Indonesia. [g]Department of Chemistry, Faculty of Mathematics and Natural Sciences, University of Nusa Cendana, Kupang, East Nusa Tenggara, (85001), Indonesia. [h]Department of Cemistry, Faculty of Mathematics and Natural Sciences, Gorontalo State University, Gorontalo (96119), Indonesia. *Corresponding author. E-mail: **boybaunsele@mail.com**

The research employs a range of state-of-the-art laboratory instruments, including a Fourier Transform Infrared (FTIR) spectrophotometer (Thermo Scientific Nicolet iS10), a scanning electron microscopy (SEM) (brand JSM-6510LA), a pH meter (Metler Toledo and PH-009 (I) A), a universal pH indicator, an 80-mesh sieve, an analytical balance (Meter AE 200 and Acis AD 300H), and a drying oven.

2.2 Biosorbent Preparation

Teak wood sawdust was systematically collected from furniture production, followed by a purification process to eliminate any contaminants. The material was then finely ground using a mortar and subsequently sieved through an 80-mesh screen to achieve uniform particle size. The resulting fine powder was thoroughly rinsed with distilled water to remove any residual impurities. Finally, the cleaned material was dried in an oven at 80°C for 2 hours to ensure consistent moisture removal and sample stability before further analysis [30].

2.3 Biosorbent Characterization

The characterization of biosorbents was conducted using several analytical methods, including the determination of the pH zero-point charge (pH_{pzc}), as well as Fourier Transform Infrared (FTIR) spectroscopy and Scanning Electron Microscopy (SEM) and Energy Dispersive X-ray Spectroscopy (EDX) analyses. The pH_{zpc} was performed by using salt addition method. Briefly, eight containers, each containing 20 mL of 0.1 M NaCl, were prepared. The initial pH of the solutions was adjusted across a range of 3 to 10 using standardized NaOH and HCl solutions. Subsequently, 0.1 g of teak sawdust was introduced into each container, and the mixtures were stirred for 30 minutes to ensure proper dispersion. The suspensions were then allowed to equilibrate at room temperature for 24 hours. After the equilibration period, the final pH of each solution was measured. The pH_{pzc} was identified by plotting the initial pH (pH_i) against the corresponding change in pH ($\Delta pH = pH_i - pH_f$), with the pH_{pzc} value corresponding to the point at which ΔpH equals zero [30].

FT-IR spectra were acquired on a Thermo Scientific Nicolet iS10 spectrometer (DTGS detector, KBr beamsplitter) using the KBr-pellet technique. Oven-dried teak sawdust was finely ground, mixed with spectroscopic-grade KBr at approximately 1:100 (w/w), and pressed into 13 mm pellets using a hydraulic press (~8–10 ton, ~60 s). FT-IR spectra were recorded over the 4000–500 cm^{-1} range at a spectral resolution of 4 cm^{-1}. Characteristic bands enabled the identification of key functional groups, such as O–H stretching at 3200–3600 cm^{-1} and C=O stretching at 1600–1700 cm^{-1}. A KBr background was recorded immediately prior to each measurement under identical conditions; the sample compartment was purged with dry air to minimize atmospheric H_2O/CO_2 bands. The FT-IR analysis results are presented in Figure 2.

Surface morphology was examined by SEM (JSM-6510LA, JEOL Ltd., Tokyo, Japan) in high-vacuum mode using the secondary-electron (SE) detector at an accelerating voltage of 15 kV and a working distance of 10 mm. Oven-dried powders were mounted on aluminum stubs with conductive carbon tape and sputter-coated with Au/Pd (~5 nm) prior to imaging. Micrographs were acquired at 1,000–3,000×. Elemental analysis was performed with the integrated JEOL JED-2300 EDS (SDD); spectra were collected at 15 kV, 60 s live time, and 20–30% dead time from three representative areas per sample, and quantified by the instrument's standardless ZAF routine for C, N, O, and Cl; results are summarized in Figure 4 and Figure 5.

2.4 Solution Preparation

A 100 ppm methylene blue (MB) stock solution was prepared by dissolving 100 mg of MB powder in a 1000 mL volumetric flask, followed by thorough shaking to ensure homogeneity. This stock solution was subsequently used in the adsorption experiments. To determine the maximum absorbance wavelength (λ max), the stock solution was diluted to a concentration of 5 ppm, and its absorbance was recorded within the 600–700 nm range using a UV-Vis spectrophotometer. The λ max value obtained was then used for all subsequent absorbance measurements. For the calibration curve, a series of MB standard solutions with concentrations ranging from 2 to 10 ppm were prepared from the stock solution. The absorbance of each was measured at the determined λ max, and the resulting data were used to construct a calibration curve and derive the corresponding linear regression equation.

2.5 Determination of Optimum Adsorption pH

A total of eight containers were each filled with 20 mL of 10 ppm MB each and the pH of each was adjusted sequentially to 3, 4, 5, 6, 7, 8, 9, and 10. Subsequently, 0.1 g of teak sawdust biosorbent was added to each container and the mixture was shaken for 75 minutes, following the procedure outlined in previous research [31]. Each test was conducted once without replication. After the designated contact time of 75-minute mark, the mixture was filtered and the resulting filtrates were analyzed using UV-Vis spectrophotometer to determine the residual MB concentration. The pH condition of the MB solution yielding the highest adsorption capacity was identified based on the analysis of the adsorption data.

2.6 Determination of Optimum Contact Time

A series of eight containers, each containing 20 mL of 10 ppm MB solution adjusted to previously determined optimum pH, were prepared to evaluate the effect of contact time on the adsorption. To each container, 0.1 g of biosorbent was added, followed by the agitation for varying duration contact times of 5, 10, 20, 30, 45, 60, 75, and 90 minutes. After each contact time was achieved, the mixtures were filtered, and the filtrates were analyzed using UV-Vis spectrophotometry to determine the residual concentration of MB in each solution. The percentage of MB removal was calculated using Equation (1), while the adsorption capacity at equilibrium (q_e) was determined using Equation (2).

$$\%\ adsorption = \frac{(Co-Ce)}{Co}\ x\ 100\% \qquad (1)$$

$$q = \frac{(Co-Ct)v}{m} \qquad (2)$$

Here, C_o represents the initial concentration of methylene blue (MB) before adsorption, while C_e denotes the equilibrium concentration after adsorption. C_t refers to the concentration of MB at a specific time during the adsorption process. The parameter v indicates the volume of MB solution (L), and m represents the mass of the teak sawdust biosorbent (g). Additionally, q denotes the adsorption capacity of the adsorbent, expressed in mg g^{-1}, which quantifies the amount of adsorbate retained per unit mass of the biosorbent [32].

The data obtained from the contact time variation experiments were then used to determine the kinetics of MB adsorption onto the teak sawdust biosorbent. Kinetic

modeling was conducted using four commonly applied adsorption kinetic models, as summarized in Table 1 [33]. Among these models, the one exhibiting the highest coefficient of determination (R^2) (value closest to one) is considered to best describe the adsorption behavior of MB onto the teak sawdust biosorbent [34].

Table 1. Mathematical equation models for MB adsorption kinetics by biosorbent.

Kinetic model	Reaction equation	Graph plot
Pseudo-first order [35]	$\ln(qe - qt) = \ln qe - kt$	$tvs \ln(qe - qt)$
Pseudo-second order [35]	$\frac{t}{qt} = \frac{1}{kqe^2} + \frac{t}{qe}$	$t\ vs \frac{t}{qt}$
Elovich [36]	$qt = \left(\frac{1}{ß}\right)\ln(\alpha ß) + \left(\frac{1}{ß}\right)\ln t$	$qt\ vs \ln t$
Intraparticle diffusion [36]	$qt = kp\sqrt{t} + C$	$qt\ vs\sqrt{t}$

2.7. Determination of Optimum Concentration

Eight containers, each containing 20 mL solution of MB at varying initial concentrations ranging from 5 to 90 ppm were prepared. The pH of each solution was adjusted according to the previously optimized adsorption value. Subsequently, a 0.1 g of biosorbent (particle size of 80 mesh) was added to each container. The mixtures were agitated for the optimal contact time, after which the solutions were filtered to separate the biosorbent from the filtrate. The absorbance of each filtrate was measured using a UV-Vis spectrophotometer to evaluate the residual MB concentration and determine the adsorption performance at each initial concentration. The resulting data were then used to assess the most suitable adsorption isotherm model for describing MB uptake by the biosorbent. Six isotherm models, including Langmuir, Freundlich, Temkin, Harkin-Jura, Redlich-Peterson, and Jovanovic, were applied. Linearized forms of these models were constructed by plotting experimental data as summarized in Table 2, and the resulting linear equations were analysed to determine the best-fitting model.

Table 2. Isothermal Adsorption Mathematical Equation Model.

Isothermal model	Linear regression	Graph Plot
Langmuir [37]	$\frac{1}{qe} = \frac{1}{Qo} + \frac{1}{KlQoCe}$	$\frac{1}{qe} vs \frac{1}{Ce}$
Freundlich [37]	$\log qe = \log Kf + \frac{1}{n}\log Ce$	Log qe vs log Ce
Temkin [38]	$qe = ß \ln K_T + B \ln Ce$	ln Ce vs qe
Harkin-Jura [39]	$\frac{1}{qe^2} = \frac{B}{A} - \left(\frac{1}{A}\right)\log Ce$	$\frac{1}{qe^2} vs \log Ce$
Redelich-Peterson [39]	$ln\frac{Ce}{qe} = ß \ln Ce - \ln A$	$ln\frac{Ce}{qe} vs \ln Ce$
Jovanovic [39]	$\ln qe = \ln q_{max} - K_l Ce$	*ln qe vs Ce*

3. Results and Discussion

3.1 FTIR Analysis of Teak Sawdust

FTIR analysis was conducted to determine the functional groups present on the surface of teak sawdust biosorbent. The results confirmed the presence of characteristics functional groups associated with hemicellulose, lignin, and cellulose, consistent with previously reported findings [40]. Cellulose, a major component in organic matter, is known for its efficacy in adsorbing cationic dyes such as methylene blue due to its abundance of hydroxyl groups that facilitate electrostatic interactions and hydrogen bonding [41]. The data from this study, showing the results of FTIR analysis for teak sawdust, are presented in Figure 2.

The FTIR data, presented in Figure 2, reveals notable differences in functional group vibrations before and after MB adsorption. A broad spectrum observed at 3425 cm^{-1} before MB adsorption and shifted to 3371 cm^{-1} after MB adsorption correspond to the OH group stretching vibrations, characteristic of hydroxyl groups in alcohols and phenols, typically occurring within the 3600–3000 cm^{-1} range [42]. Peaks observed at 2924 and 2939 cm^{-1} indicate the presence of aliphatic C–H stretching vibrations, which are associated with –CH groups in lignocellulosic materials. After MB adsorption, a noticeable decrease in the intensity of these vibrations suggests interaction between the dye molecules and the biosorbent's surface functional groups [43]. Distinct aromatic C=C stretching vibrations are evident at 1597 and 1604 cm^{-1}, confirming the presence of aromatic structures [44]. A weak absorption peak at 1735 cm^{-1} is indicative of C=O stretching vibrations, often associated with carbonyl groups in lignin or hemicellulose components [25]. The peak observed at 1056 cm^{-1} corresponds to C–O stretching vibrations, typically originating from alcohols and ethers in cellulose molecules [45]. As seen in Figure 2, the observed reduction in intensity and sharpness of specific FTIR peaks following methylene blue (MB) adsorption suggests the occurrence of molecular interactions between MB molecules and the active functional groups present on the surface of the teak sawdust biosorbent. These spectral changes imply that the adsorption process is facilitated by chemical interactions, notably hydrogen bonding and electrostatic attractions. Such interactions are indicative of the involvement of surface hydroxyl, carbonyl, and aromatic groups in the binding of MB. Additionally, the functional groups identified in the teak sawdust are consistent with those reported in previous studies, as outlined in Table 3, thereby reinforcing the reliability of the functional characterization.

3.2. SEM Analysis of Teak Wood Sawdust

Surface morphology analysis of teak sawdust was performed using SEM and SEM-EDX techniques. SEM images were captured at 1000 and 3000 times magnification, both before and after MB adsorption, as shown in Figure 3. The biosorbent particles exhibited a predominantly small, oval

morphology, and at higher magnifications, distinct surface grooves and shaft-like structures became more apparent [32]. Post-adsorption images revealed the appearance of fine lines and surface irregularities, suggesting successful MB uptake. These morphological changes indicate the adsorption of MB molecules onto the biosorbent surface, which contributed to the altered surface texture observed after the adsorption process.

The SEM-EDX analysis in Figure 4 confirms the adsorption of methylene blue (MB) onto teak sawdust. Elemental mapping reveals atomic mass percentages of C (42.81%), N (9.88%), O (46.97%), and Cl (0.34%), indicating the presence of functional groups such as hydroxyl, carboxyl, and ester. The detection of Cl and N further supports the presence of MB, as Cl corresponds to the dye's counterion and N reflects azo groups (–N=N–), characteristic of MB's chromophores. A more detailed atomic distribution is shown in Figure 5.

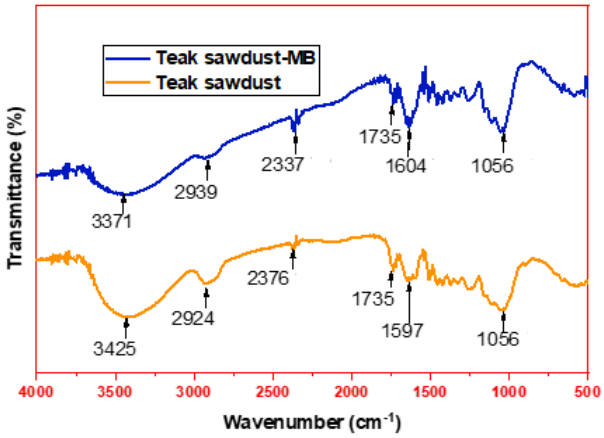

Fig. 2. FTIR spectra of teak sawdust biosorbent before and after MB adsorption.

Table 3. FTIR data for several adsorbents.

Functional groups	Wavenumber (cm^{-1})	Adsorbent
C–H; O–H; C=O	2900; 3500–3100; 1700–1600	Mushroom [46]
C–H; O–H; C=C; C–O	2939; 3296; 1608 and 817; 1267 and 1060	Coconut fiber [17]
C–H; O–H; C–O	2927; 3355; 1064	Chitosan [47]
C–H; O–H; C–C; C–O	1459 and 1377; 3370; 2923 and 2854; 1744 and 1711	Coconut pulp [48]
C–H; O–H; C–C; C=O; C–O	2918; 3433; 1629; 1431; 1162	Figs [49]
C–H; O–H; C–C	2926 and 2930; 3447 and 3412; 1423 and 1462	Moringa oleifera seed pod [30]
C–H; O–H; C=C; C=O	2926; 3433; 1624–1618; 1705–1739	Coconut husk [50]

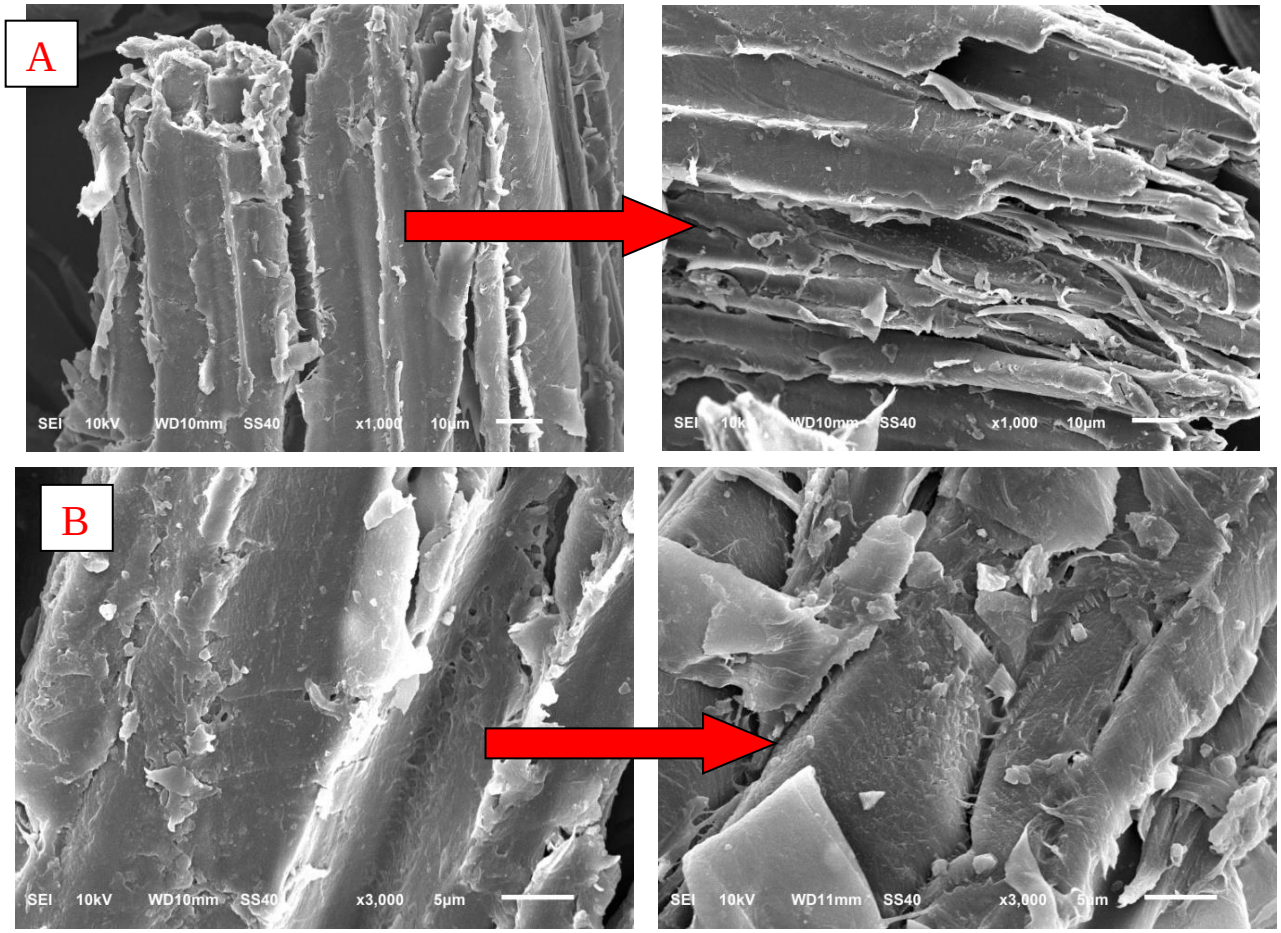

Fig. 3. SEM analysis results before and after adsorption for magnification A) 1000 times and B) 3000 times.

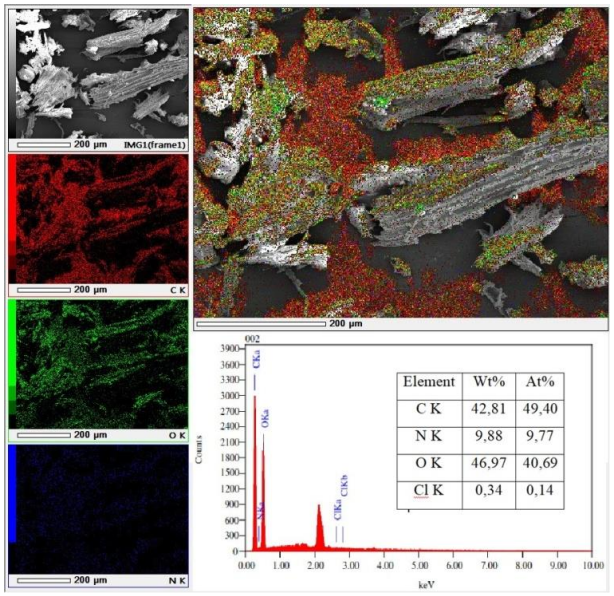

Fig. 4. SEM-EDX analysis results.

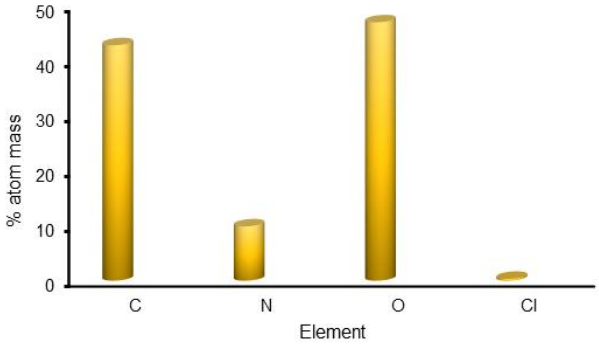

Fig. 5. Atomic distribution on the adsorbent.

3.3 pH_{pzc} Analysis of Teak Wood Sawdust

According to the data presented in Figure 6, the pH_{pzc} of the teak sawdust biosorbent is identified at pH 6, indicating that the biosorbent surface carries a net neutral charge at this pH. This condition is favorable for adsorption interactions, as minimal electrostatic repulsion occurs between the adsorbent and adsorbate at this equilibrium point [51]. When the solution pH is below the pH_{pzc}, the biosorbent surface acquires a positive charge, enhancing its affinity for anionic species [50]; however, this also results in electrostatic repulsion with cationic dyes such as methylene blue. In contrast, at pH values above the pH_{pzc}, the biosorbent surface becomes negatively charged, promoting stronger electrostatic attraction with cationic adsorbates like methylene blue, thereby improving adsorption efficiency [52].

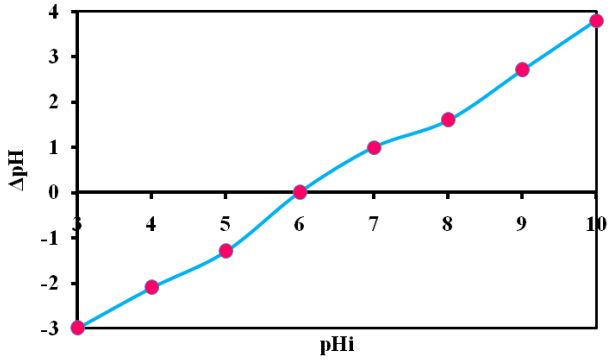

Fig. 6. Biosorbent pH_{pzc} data.

3.4. Effect of Methylene Blue pH Variations

MB is a light-sensitive compound that undergoes photodegradation when exposed to ultraviolet (UV) or visible light, primarily due to its chromophoric structure, which absorbs photon energy and initiates photochemical reactions leading to molecular breakdown. The extent of this photodecomposition is influenced by several factors, including light intensity, wavelength, exposure duration, and environmental conditions such as the presence of oxygen, catalytic agents, or radical-generating species. MB is particularly susceptible to degradation under neutral and alkaline conditions, whereas it demonstrates greater stability in acidic environments. To minimize unintended photodegradation, MB solutions were stored in dark conditions and shielded from excessive light exposure during preparation, storage, and experimental procedures.

The initial step in the adsorption study involved the determination of the maximum absorbance wavelength of MB, which was identified at 665 nm, aligned with previously reported finding [16]. Following this, a calibration curve was constructed by plotting MB concentration on the x-axis against absorbance on the y-axis, resulting in a linear regression line with a regression equation of y = 0.219x + 0.007 and a coefficient of determination (R^2) of 0.997. The resulting equation was then used to MB concentrations in the solutions in all the experiments. The standard curve, illustrated in Figure 7, served as the basis for evaluating the effect of solution pH on the adsorption capacity of the biosorbent.

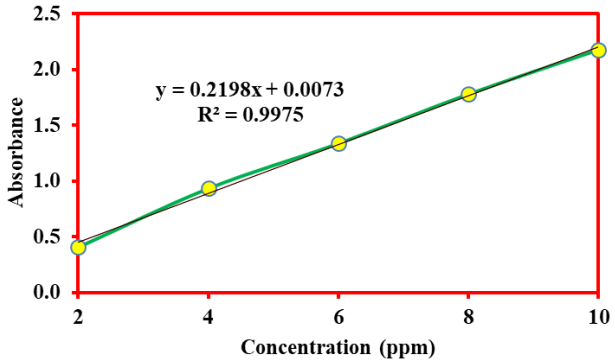

Fig. 7. Standard curve of MB adsorption.

As illustrated in Figure 8, the MB adsorption test revealed that the maximum adsorption capacity of 2.04 mg g^{-1} and the highest adsorption efficiency of 99.26% were achieved at pH 6. At pH< 6, the biosorbent surface becomes protonated, leading to a reduction in available negatively charged sites for MB adsorption. The high concentration of H^+ ions competes with cationic MB molecules for interaction with the negatively charged functional groups present in the cellulose, thereby reducing the overall adsorption efficiency. Conversely, at pH> 6, excess OH^- ions may interact with the positively charged regions of the MB molecules, hindering their ability to bind to the biosorbent's active sites. These findings are consistent with the data presented in Figure 6, which confirms that at pH 6, the biosorbent surface exhibits neutral charge characteristics, minimizing electrostatic interference and thus optimizing the interaction between MB molecules and the biosorbent's functional groups.

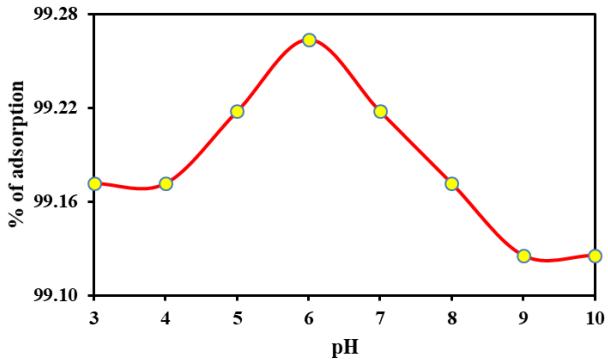

Fig. 8. Curve of the influence of variations in the pH of the MB solution on the MB adsorption capacity.

3.5. Adsorption kinetics

As illustrated in Figure 9, the optimum contact time for MB adsorption onto teak sawdust biosorbent was determined to be 30 minutes, yielding adsorption capacity of (qt) of 2.045 mg g^{-1} and a removal efficiency of 99.4%. Figure 9 also shows that the adsorption capacity steadily increases between 5 and 30 minutes, likely due to the availability of numerous active sites on the biosorbent surface facilitating interaction with MB molecules. Once these active sites become increasingly occupied, the adsorption rate begins to level off. Beyond the 30-minute mark, no significant increase in adsorption was observed, suggesting that the biosorbent surface may have reached saturation, thereby limiting further interactions between MB and the adsorbent. These findings confirm that 30 minutes represents the equilibrium point for maximum adsorption under the studied conditions.

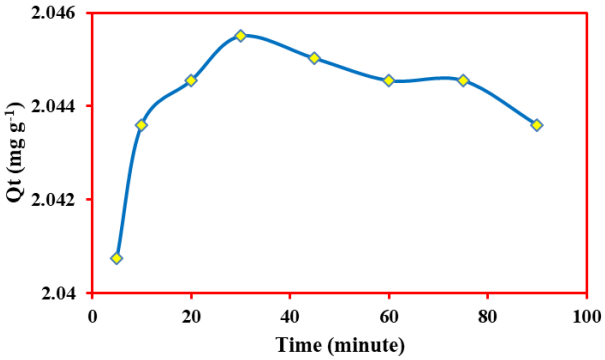

Fig. 9. Effect of varying contact time on MB adsorption capacity.

Table 4. Kinetic parameters of MB adsorption by teak sawdust

Models	Kinetic parameters
pseudo-first order	K_1 (0.000000009 min^{-1}) Qe (18.52 mg g^{-1}) R^2 (0.7129)
pseudo-second order	K_2 (79.71 min^{-1}) Qe (2.004 g mg^{-1}) R^2 (1)
Elovich	ß (0.000218 g mg^{-1}) α (5623,48 mg g^{-1} min^{-1}) R^2 (0,434)
Intraparticle diffusion	Kp (896.6) C (1826) R^2 (0.253)

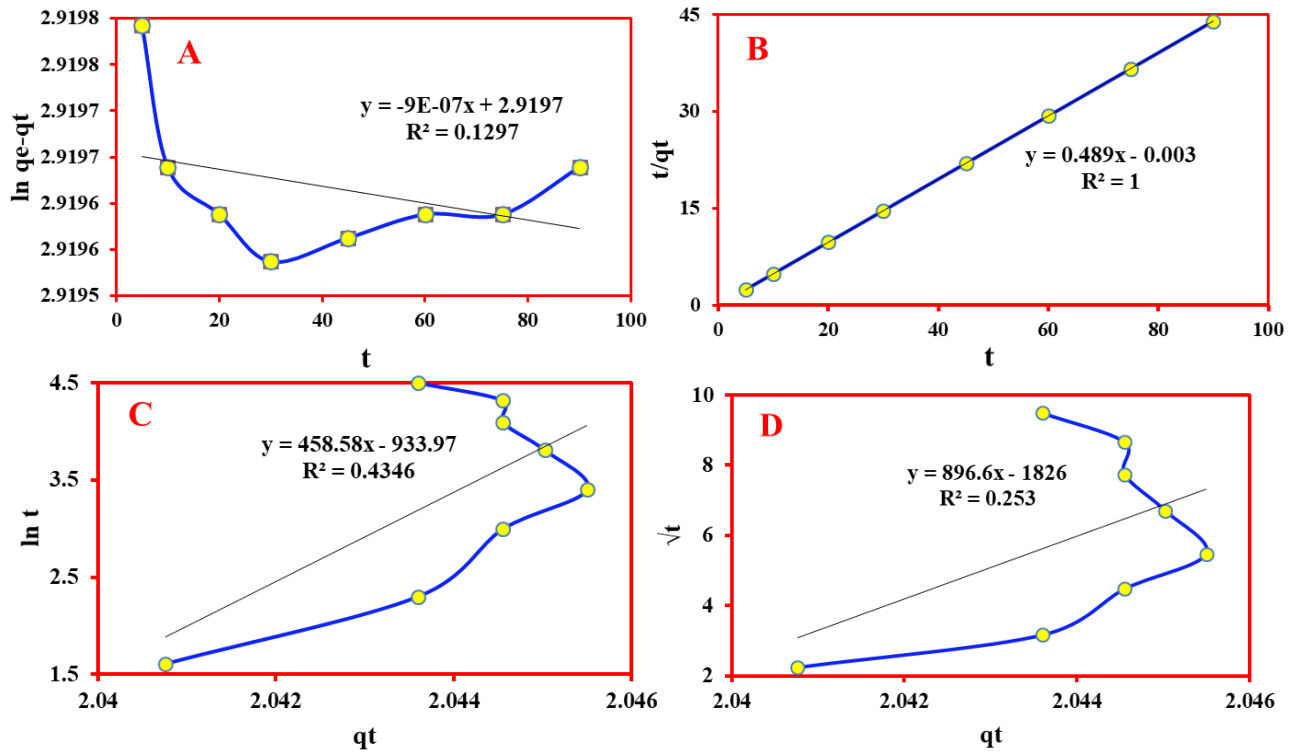

Fig. 10. Adsorption kinetic model, A) pseudo-first-order; B) pseudo-second-order; C) Elovich; D) intraparticle diffusion.

According to the data presented in Table 4, the pseudo-second-order adsorption kinetic model yielded the highest coefficient of determination (R^2), suggesting the best fit among the four kinetic models evaluated. This indicates that the adsorption rate of the MB adsorbate is primarily governed by chemisorption mechanisms, which depend on the interaction between the adsorbate molecules and the available active sites on the biosorbent surface [53]. The experimentally measured MB adsorption capacity of 2.045 mg g^{-1} closely approximates theoretical maximum adsorption capacity of 2.004 mg g^{-1} calculated using the pseudo-second-order kinetic equation. This small deviation further supports the model's validity, highlighting the role of active site availability in the adsorption process. These findings are consistent with previous studies on dye adsorption using lignocellulosic biosorbents, which also conform to pseudo-second-order kinetics, as summarized in Table 5.

Table 5. Pseudo-second-order kinetic data for several biosorbents against dyes

Biosorbent	Dye	R^2
Coconut coir [16]	Methylene Blue	1
Mangrove sap [13]	Methylene Blue	0.999
Coconut coir [54]	Rhodamine B	0.9871
Moringa oleifera seed pot [30]	Rhodamine B	0.999
Bagasse [53]	Methylene Blue	0.999
Eucalyptus powder [55]	Methylene Blue	0.999
Chinar leaves [56]	Methylene Blue	1
Dry leaf trash [57]	Methylene Blue	0.99
Coconut bunches [58]	Methylene Blue	0.99
Clove leaves [22]	Methylene Blue	0.99
This study	Methylene Blue	1

3.6 Adsorption isothermal

The adsorption process begins with the migration of the adsorbate molecules towards the surface of the adsorbent, where they interact with active functional groups and subsequently diffuse into the porous structure of the biosorbent [9]. To investigate the influence of varying adsorbate (MB) concentrations, the MB concentration was varied between 5 to 90 ppm, under optimized conditions of pH 6 and 30 minutes contact time. Based on the data presented in Figure 11, the maximum adsorption capacity was obtained at 30 ppm, corresponding to a removal efficiency of 99.79%. At concentrations ranging from 5 to 30 ppm, the increase in the adsorption efficiency can be attributed to the abundance of unoccupied active sites on the teak sawdust surface, which readily interact with MB molecules. In this concentration range, the number of available active sites surpasses the number of MB molecules. However, at concentrations above 30 ppm, a decline in adsorption capacity was observed, likely due to the saturation of adsorption sites, which limits further uptake of MB. This saturation effect suggests the formation of a monolayer of dye molecules on the biosorbent surface, thereby inhibiting additional adsorption [25].

In this study, six isotherm models were employed to investigate the adsorption behaviour of MB onto the teak sawdust, as listed in Table 2. Linear regression analysis was conducted to determine the correlation coefficients (R^2) of each model. The corresponding isotherm parameters are summarized in Table 6, while the linear regression plots are presented in Figure 12. Based on the comparative analysis of R^2 values in Table 6, it was concluded that the isotherm model with the highest R^2 closest to unity most accurately represents the adsorption equilibrium of MB onto the teak sawdust biosorbent.

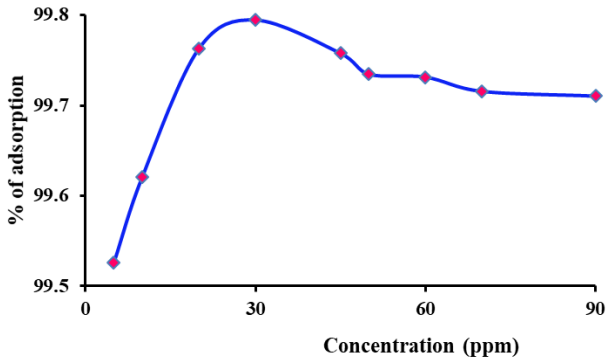

Fig. 11. Effect of variations in MB concentration.

Table 6 presents the R^2 values for the isothermal adsorption of MB using six models: Langmuir, Freundlich, Temkin, Harkin-Jura, Redelich-Peterson, and Jovacovic. Among these, the Langmuir and Freundlich models yielded the highest R^2 values (closest to 1), suggesting the best fit for the experimental data. These results demonstrate that the adsorption of MB onto teak sawdust occurs through a combination of chemisorption [43] and physisorption [55]. The applicability of the Langmuir model implies monolayer adsorption, in which each active site on the biosorbent surface is occupied by a single MB molecule. This model assumes uniform adsorption energies across the surface and no interaction between adsorbed molecules, reflecting a balance between the number of available adsorption sites and MB molecules in the system [59].

Table 6. Isothermal adsorption parameters

Isotherm models	Parameter	value
Langmuir	Qmax (mg g^{-1})	2
	KL (L mol^{-1})	159925
	E (kJ mol^{-1})	35.392
	R^2	1
Freundlich	Kf (mg g^{-1})	1.351
	n	1
	R^2	1
Temkin	B	0.015
	A	$2.68x10^{50}$
	R^2	0.868
Harkin-Jura	A	0.009443
	B	0.005716
	R^2	0.701
Redelich-Peterson	Kr (L g^{-1})	116.39
	ß	20.66
	R^2	0.972
Jovanovic	Kj	55.05
	qmax (mg g^{-1})	4.56×10^{-46}
	R^2	0.868

The findings presented in Figure 9 suggest that after 30 minutes of contact time, no further increase in methylene blue (MB) adsorption was observed. In fact, a plateau or slight decline in adsorption capacity suggests potential physical desorption or equilibrium saturation, which is characteristic of physisorption. This behaviour aligns with the Freundlich isotherm model, which accounts for multilayer adsorption on

heterogeneous surfaces [60]. The porous structure of the teak sawdust biosorbent, as illustrated in Figure 3, further supports this mechanism. Although both the Langmuir and Freundlich models exhibited similarly high R^2 values, the Freundlich constant (n) value of 1 falls within the favourable range (1–10), indicating a good fit with the Freundlich model [61]. Additionally, the Freundlich adsorption capacity constant (Kf) of 1.351 mg g^{-1} implies that 1 gram of teak sawdust can adsorb approximately 1.351 mg of MB within a 30-minute contact time under the given conditions.

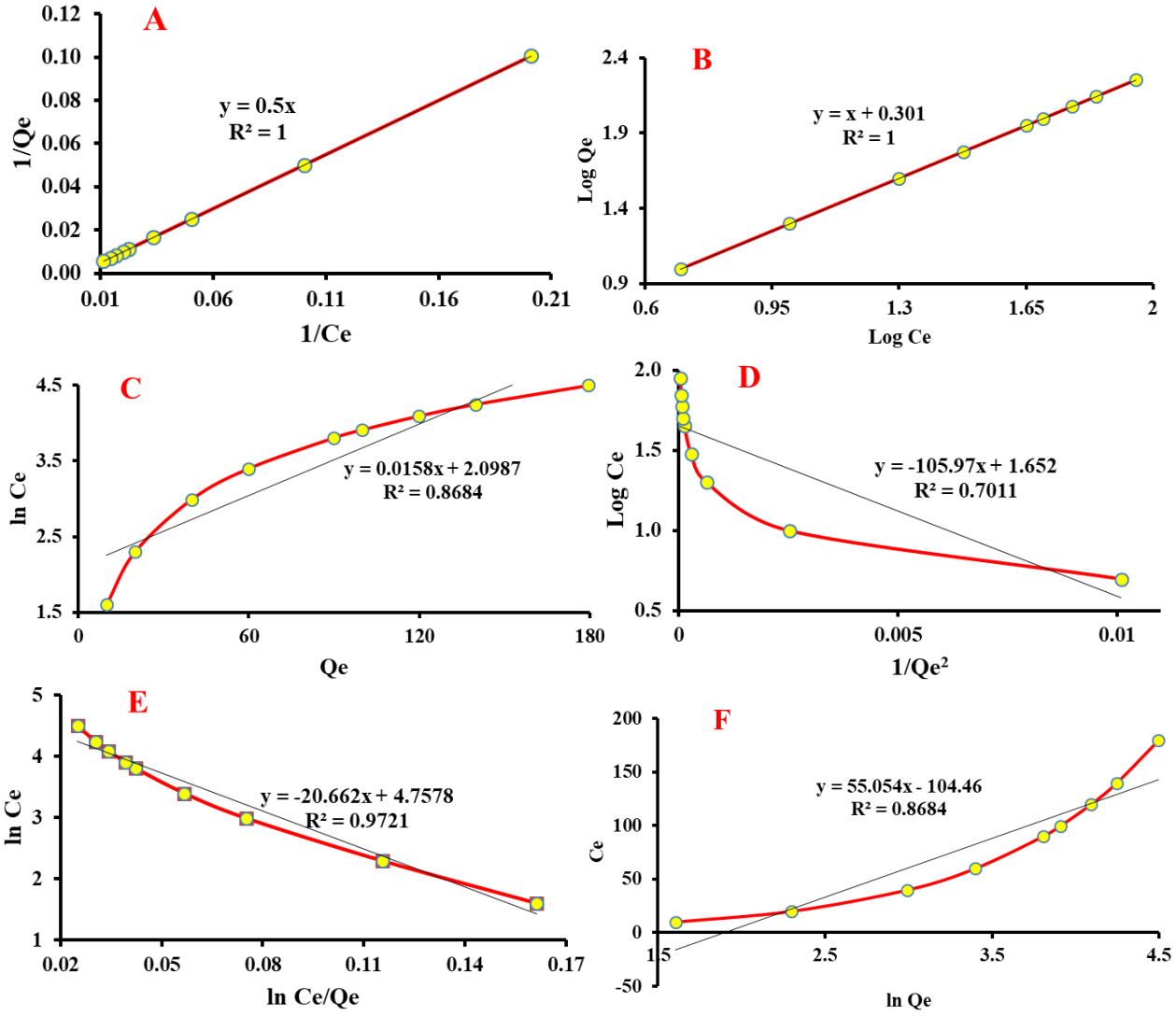

Fig. 12. Adsorption isothermal graph plot: A) Langmuir; B) Freundlich; C) Temkin; D) Harkin-Jura; E) Redelich-Peterson; and F) Jovacovic.

4. Conclusions

The findings of this study strongly underscore the potential of teak sawdust, an abundant byproduct of carpentry industry, as an efficient and environmentally friendly biosorbent for methylene blue removal from wastewater. Its high adsorption capacity (1.351 mg g^{-1}) and remarkable efficiency (99.79%) indicate that this material could serve as a viable option for water treatment applications. Additionally, the adsorption process follows a pseudo-second-order kinetic model, suggesting that chemisorption plays a dominant role due to the strong interactions between methylene blue molecules and the functional groups present in teak sawdust. From a sustainability perspective, the use of teak sawdust as a biosorbent offers a dual benefit—reducing dye pollution while repurposing industrial waste. Unlike conventional chemical treatments that may introduce secondary pollutants, this approach relies on a naturally available, biodegradable material. Moreover, the study highlights the importance of optimizing adsorption parameters, such as pH, contact time, and dye concentration, to enhance efficiency, making it adaptable for real-world wastewater treatment scenarios. Overall, this research demonstrates the feasibility of teak sawdust as a cost-effective and sustainable alternative to synthetic adsorbents, contributing to the advancement of greener water treatment technologies. However, further studies are necessary to evaluate its regeneration potential and effectiveness in treating more complex wastewater systems.

Acknowledgments

This research was supported by the Widya Mandira

Catholic University Research and Service Institute (LPPM) through the Regular Research Grant program.

Author Contributions

Conceptualization, A. B. B., J. N. N., D.S.; Methodology, A. B. B., F. N., Investigation and Formal Analysis, A. B. B., M. N., D.S.; Software, A. B. B.; Resources, A. B. B., H. M.; Supervision, D. S., J. N. N., A. T. L; Validation, D.S., F. N.; Visualization, A. B. B., H. M., F.N.; Writing – Original Draft, A. B. B.; Writing – Review and Editing, A. B. B., H. M., F. N., A. T. L., J. L. K.

References and Notes

[1] Rahayu, R.; Nurlette, S.; Baunsele, A. B. *Stannum: Jurnal Sains Dan Terapan Kimia* **2023**, *5,* 78. [Crossref]

[2] Exley, J. M.; Hunter, T. N.; Pugh, T.; Tillotson, M. R. *Powder Technol.* **2023**, *421*, 118387. [Crossref]

[3] Lellis, B.; Fávaro-Polonio, C. Z.; Pamphile, J. A.; Polonio, J. C. *Biotechnology Research and Innovation* **2019,** *3*, 275. [Crossref]

[4] Afrin, S.; Shovu, H. R.; Sultana, B.; Islam, F.; Rus'd, A. A.; Begum, S.; Hossain, M. S. *Heliyon* **2021**, *7*, 08102. [Crossref]

[5] Zein, R.; Purnomo, J. S.; Ramadhani, P.; Safni, A. M. F.; Putri, C. N. *Arabian J. Chem.* **2023**, *16*, 104480. [Crossref]

[6] Handayani, S. N.; Irmanto, I.; Indriyani, N. N. *Molekul* **2023,** *18*, 107. [Crossref]

[7] Jumaeri, J.; Nadiyya, A.; Prasetya, A. T.; Sumarni, W. *J. Kim. Sains Apl.* **2022**, *25*, 205. [Crossref]

[8] Hardian, A.; Rosidah, R.; Budiman, S.; Syarif, D. G. *J. Kim. Sains Apl.* **2021**, *23*, 440. [Crossref]

[9] Staroń, P.; Chwastowski, J.; Banach, M. *Int. J. Environ. Sci. Technol.* **2019**, *16*, 8449. [Crossref]

[10] Kumar, M. S.; Supraja. N.; David, E. *Novel Research in Science* **2019**, 2. [Crossref]

[11] Talaiekhozani, A.; Mosayebi, M. R.; Fulazzaky, M. A.; Eskandari, Z.; Sanayee, R. *Alexandria Eng. J.* **2020**, *59*, 549. [Crossref]

[12] Riyanto, M. M. *IOSR J. Appl. Chem.* **2015**, *8*, 31. [Crossref]

[13] Azis, T.; Ahmad, L. O.; Awaliyah, K.; Kadir, L. A. *J. Kim. Sains Apl.* **2020**, *23*, 370. [Crossref]

[14] Ashik, A. A.; Rahman, M. A.; Halder, D.; Hossain, M. M. *Appl. Water Sci.* **2023**, *13*, 81. [Crossref]

[15] Utomo, H. D.; Phoon, R. Y. N.; Shen, Z.; Ng, L. H.; Lim, Z. B. *Nat. Resour.* **2015**, 6. [Crossref]

[16] Baunsele, A. B.; Boelan, E. G.; Kopon, A. M.; Rahayu; S. D. *Indonesian Journal of Chemistry Research* **2022**, *10*, 110. [Crossref]

[17] Baunsele, A. B.; Missa, H. *Walisongo Journal of Chemistry* **2021**, *4*, 131. [Crossref]

[18] Baunsele, A. B.; Kopon, A. M.; Boelan, E. G.; Leba, M. A. U.; Komisia, F.; Tukan, M. B.; Taek, M. M.; Tukan, G. D.; Missa, H.; Siswanta, D.; Naat, J. N.; Rahayu. *Molekul* **2024**, *19*, 128. [Crossref]

[19] Banamtuan, T. E.; Baunsele, A. B.; Kopon, A. M. *Jurnal Inovasi Teknik Kimia* **2023,** 8. [Link]

[20] Ninu, Y. D.; Baunsele, A. B. *SPIN Jurnal Kimia dan Pendidikan Kimia* **2023**, *5*. [Crossref]

[21] Sylvia, N.; Dewi, R.; Zulnazri, Z.; Setiawan, H.; Humaira, D.; Reza, M. *J. Kim. Sains Apl.* **2023**, *26*, 310. [Crossref]

[22] Kusuma, H. S.; Aigbe, U. O.; Ukhurebor, K. E.; Onyancha, R. B.; Okundaye, B.; Simbi, I.; Ama, O. M.; Darmokoesoemo, H.; Widyaningrum, B. A.; Osibote, O. A.; Balogun, V. A. *Results Chem.* **2023**, *5*, 100778. [Crossref]

[23] Fang, J.; Gao, B.; Mosa, A.; Zhan, L. *Chem. Speciation Bioavailability* **2017**, *29*, 197. [Crossref]

[24] Sousa, V. B.; Cardoso, S.; Quilhó, T.; Pereira, H. *Rev. Biol. Trop.* **2012**, 60. [Crossref]

[25] Mishra, Y.; Sowmya, V.; Shanthakumar, S. *Journal of Urban and Environmental Engineering* **2015**, *9*, 102. [Crossref]

[26] Yusop, M. F. M.; Aziz, A.; Ahmad, M. A. *Arabian J. Chem.* **2022**, *15*, 104081. [Crossref]

[27] Yusop, M. F. M.; Khan, M. N. N.; Zakaria, R.; Abdullah, A. Z.; Ahmad, M. A. *Arabian J. Chem.* **2023**, *16*, 104780. [Crossref]

[28] Younis, H. M.; Hussein, H. A.; Khaphi, F. L.; Saeed, Z. K. *Heliyon* **2023**, *9*, 21698. [Crossref]

[29] Chayaporn, P.; Sasaki, N.; Venkatappa, M.; Abe, I. *Cleaner Environmental Systems* **2021**, *2*, 100023. [Crossref]

[30] Bello, O. S.; Lasisi, B. M.; Adigun, O. J.; Ephraim, V. *Chem. Speciation Bioavailability* **2017**, *29*, 120. [Crossref]

[31] Baunsele, A. B.; Missa, H. *Akta Kimia Indonesia* **2020**, *5*, 76. [Crossref]

[32] Nipa, S. T.; Shefa, N. R.; Parvin, S.; Khatun. M. A.; Alam, M. J.; Chowdhury, S.; Khan, M. A. R.; Shawon, S. M. A. Z.; Biswas, B. K.; Rahman, M. W. *Results Eng.* **2023**, *17*, 100857. [Crossref]

[33] Lima, É. C.; Adebayo, M. A.; Machado, F. M. *Carbon Nanomaterials as Adsorbents for Environmental and Biological Applications* **2015,** 33. [Crossref]

[34] Parushuram, N.; Ranjana, R.; Harisha, K. S.; Shilpa, M.; Narayana, B.; Neelakandan, R.; Sanggapa, Y. *J. Dispersion Sci. Technol.* **2022**, *43*, 1161. [Crossref]

[35] Abbou, B.; Lebkiri, I.; Ouaddari, H.; Elkhattabi, O.; Habsaoui, A.; Lebkiri, H.; Rifi, E. H. *J. Turk. Chem. Soc., Sect. A,* **2021**, *8*, 677. [Crossref]

[36] Yakout, A. A.; Shaker, M. A.; Elwakeel, K. Z.; Alshitari, W. *J. Dispersion Scie. Technol.* **2019**, *40*, 707. [Crossref]

[37] Neolaka, Y. A. B.; Lawa, Y.; Naat, J. N.; Riwu, A. A. P.; Iqbal, M.; Darmokoesoemo, H.; Kusuma, H. S. *J. Mater. Res. Technol.* **2020**, *9*, 6544. [Crossref]

[38] Ahmad, M. A.; Ahmed, N. B.; Adegoke, K. A.; Bello, O. S. *Chem. Data Collect.* **2019**, *22*, 100249. [Crossref]

[39] Ayawei, N.; Ebelegi, A. N.; Wankasi, D. *Journal of Chemistry* **2017**, *2017*, 1. [Crossref]

[40] Trisanti, P. N.; Rifan, M.; Akbar, P.; Gunardi, I.; Sumarno, S. Isolation of cellulose from teak wood using hydrothermal method," presented at the 4TH International Seminar on Chemistry, Surabaya, Indonesia, 2021, 020047. [Crossref]

[41] Hina, K.; Zou, H.; Qian, W.; Zuo, D.; Yi, C. *Cellulose* **2018**, *25*, 607. [Crossref]

[42] Gorgieva, S.; Vogrinčič, R.; Kokol, V. *J. Polym. Environ.* **2019**, *27*, 318. [Crossref]

[43] Acut, E.; Anorico, N. F.; Acut, D. *Orbital: Electron. J. Chem.* **2023**, *15*, 186. [Crossref]

[44] Ngankam, E. S.; Dai-Yang, L.; Debina, B.; Baçaoui, A.; Yaacoubi, A.; Rahman, A. N. *Mater. Sci. Appl.* **2020**, 11. [Crossref]

[45] Kandil, H.; Ali, H. *J. Polym. Environ.* **2023**. *31*, 1456. [Crossref]

[46] Yildirim, A.; Acay, H.; *J. Turk. Chem. Soc., Sect. A* **2020**, *7*, 295. [Crossref]

[47] Grząbka-Zasadzińska, A.: Ratajczak, I.: Król, K.: Woźniak, M.: Borysiak, S. *Cellulose*, **2021**, *28*, 5745. [Crossref]

[48] Kamari, A.; Yusoff, S. N. M.; Abdullah, F.; Putra, W. P. *J. Environ. Chem. Eng.* **2014**, *2*, 1912. [Crossref]

[49] Pathania, D.; Sharma, S.; Singh, P. *Arabian J. Chem.* **2017**, 10, 1445. [Crossref]

[50] Bello, O. S.; Adegoke, K. A.; Fagbenro, S. O.; Lameed, O. S. *Appl. Water Sci.* **2019**, *9*, 189. [Crossref]

[51] Moirana, R. L.; Mkunda, J.; Machunda, R.; Paradelo, M.; Mtei, K. *Environ. Adv.* **2023**, *11*, 100329. [Crossref]

[52] Al-Maliky, E. A.; Gzar, H. A.; Al-Azawy, M. G. *IOP Conf. Ser.: Mater. Sci. Eng.* **2021**, *1184*, 012004. [Crossref]

[53] De Oliveira, F. M.; De Sousa, P. A. R.; De Melo, E. I.; Coelho, L. M. *Orbital: Electron. J. Chem.* **2020**, *12*, 76. [Crossref]

[54] Bello, O. S.; Adegoke, K. A.; Fagbenro, S. O.; Lameed, O. S. *Appl. Water Sci*. **2019**, *9*, 189. [Crossref]

[55] Esmaeili, H.; Foroutan, R. *J. Dispersion Sci. Technol.* **2019**, *40*, 990. [Crossref]

[56] Khan, F. A.; Mushtaq, M. A. B.; Arif, P. M. A.; Mazahar, M. F. *Orbital: Electron. J. Chem.* **2023**, *15*, 163. [Crossref]

[57] Gong, L.; Sun, W.; Kong, L. *Computational Water, Energy, and Environmental Engineering* **2013**, *2,* 13. [Crossref]

[58] Hameed, B. H.; Mahmoud, D. K.; Ahmad, A. L. *J. Hazard. Mater.* **2008**, *158*, 65. [Crossref]

[59] El-Bery, H. M.; Saleh, M.; El-Gendy, R. A.; Saleh, M. R.; Thabet, S. M. *Sci. Rep.* **2022**, *12*, 5499. [Crossref]

[60] Campos, A. F. C.; Silva, F. N. D.; Almeida, M. R. B. D.; Sales, L. C. A.; Michels-Brito, P. H.; Oliveira, H. A. L. D. *Orbital: Electron. J. Chem.* **2019**, *11*, 64. [Crossref]

[61] Jirekar, D.; Ubale, M.; Farooqui, M. *Orbital: Electron. J. Chem.* **2016**, *8*, 282. [Crossref]

How to cite this article

Baunsele, A. B.; Siswanta, D.; Missa, H.; Nitsae, M.; Naat, J. N.; Lema, A. T.; Nitti, F.; La Kilo, J. *Orbital: Electronic J. Chem*. **2025**, *17*, 415. DOI: http://dx.doi.org/10.17807/orbital.v17i5.20094